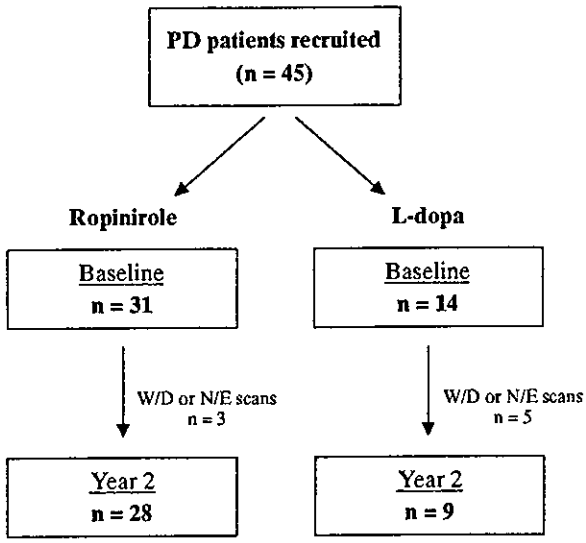

Fig. 1. Flow chart of PD ^{18}F-dopa PET Trial: PD patient subgroup numbers at baseline and 2 years (*W/D* withdrawn; *N/E* non-evaluable scan)

2-Year follow-up results

The mean percentage decreases in putamen Ki^o over 2 years were 13% and 18% for the intention-to-treat (ITT) ropinirole and L-dopa groups, respectively (Table 1). These were not significantly different and there was also no significant difference between the ropinirole and L-dopa groups when mean percentage decreases in best putamen Ki^o side only (17% versus 22%, respectively) or worst putamen Ki^o side only (4% versus 13%, respectively) were considered.

The mean subscale motor UPDRS scores at baseline and two years were 14.0 and 25.5, respectively, in the ropinirole group and 11.0 and 19.3 in the L-dopa group. Over the 2-year period, the mean increase in disability, as assessed by the UPDRS motor score in a practically-defined "off" state 12 hours withdrawn from medication, was greater for the ropinirole group (11.4 $\pm$ 1.4) than for the L-dopa group (8.2 $\pm$ 2.7), $p < 0.01$. The side with the worst

Table 1. Mean percentage changes in putamen Ki^o for each patient group at 2 years

2 Year results Intention-to-treat groups	Ropinirole	L-dopa	Difference (ropinirole-L-dopa)
	n = 28	n = 9	
Mean % change			
Averaged putamen Ki^o	−13.0 (SD 3.8)	−17.8 (SD 4.9)	4.8 p = 0.47
Best putamen Ki^o	−17.4 (SD 4.2)	−22.0 (SD 5.3)	4.6 p = 0.56
Worst putamen Ki^o	−3.6 (SD 5.0)	−13.2 (SD 5.0)	9.7 p = 0.33

putamen Ki^o at baseline was consistently contralateral to the clinically most affected limb.

Discussion

We have employed serial ^{18}F-dopa PET to measure the rate of loss of dopamine terminal function in early Parkinson's disease, over a 2-year period, in patients randomized to either ropinirole or L-dopa monotherapy. At 2 years, we were unable to demonstrate a significant difference in disease progression, as measured by loss of putamen ^{18}F-dopa uptake, between the ropinirole and L-dopa ITT groups.

Methodological issues

While ^{18}F-dopa PET enables dopamine terminal function in PD to be measured in vivo, there are several methodological issues in our trial that need to be addressed:

1) The combination of PET data acquired in 2D and 3D mode.
2) The possible effects of medication on striatal ^{18}F-dopa uptake.
3) The assumption that serial ^{18}F-dopa PET represents a valid measure of PD progression.

Acquiring datasets in 3D compared with 2D mode results in greater sensitivity and higher spatial resolution after reconstruction. This produces an overall improvement in image quality (Rakshi, 1996, 1999; Trebossen, 1996) The 3D approach, however, is more complex to reconstruct and scatter correction is problematic (Badawi, 1997; Bailey, 1994). Using the 3D approach, our current test–retest variability in putamen Ki^o for five normal subjects showed a mean variation of 2.5% (range 2–4%) (Weinhard, 1998), compared with a mean reported variation of 8% with 2D PET (Morrish, 1996; Vingerhoets, 1996). Our trial, however, required the combination of data obtained serially in 2D mode with an ECAT 931 camera for 17 patients and in 3D mode with an ECAT 953 camera for 20 patients. To address this issue, we effectively normalized for scanner differences by considering percentage changes in mean putamen Ki^o across patient groups rather than reporting absolute Ki^o changes. Furthermore, ANOVA with scanner type (2D or 3D) as a covariate did not show any effect of this variable on percentage loss of dopaminergic function at 2 years.

Another important consideration is the effect of levodopa administration on ^{18}F-dopa uptake in PD. We have studied the acute effect of levodopa administration on ^{18}F-dopa uptake in four PD subjects with established disease who had been taking L-dopa for variable periods of time. We scanned the subjects twice, one month apart, on one occasion taking 100 mg levodopa medication and on the other, off levodopa, 12 hrs prior to their PET scan. We found no significant effect on ^{18}F-dopa uptake of acute administration of L-dopa (R. Ceravalo, unpublished observations). The longterm effects of chronic levodopa therapy on ^{18}F-dopa uptake in PD are, however, unknown. Interestingly, one subject in our study did not have PD and was randomised to L-dopa during the two year trial period. He had two normal ^{18}F-dopa PET

studies with putamen Ki^{o} values in the high normal range. Although we cannot assume that chronic levodopa exposure does not alter ^{18}F-dopa uptake in PD, it is nevertheless reassuring that in non-parkinsonian subjects this does not appear to be an issue (Turjanski, 1999).

It could be argued that dopamine agonists may also affect ^{18}F-dopa uptake by down-regulating dopa decarboxylase (DDC) activity, although there is currently no evidence to support this. If that were the case we would have expected a relatively greater reduction in ^{18}F-dopa uptake in the ropinirole compared with the L-dopa group; this was not observed in our study. Further studies are clearly required to determine whether chronic exposure to dopaminergic agents alters DDC activity. Preliminary data (N. Pavesi, unpublished) suggests that dopamine agonists, at least in non-parkinsonian states (e.g. Restless Legs Syndrome), does not reduce striatal ^{18}F-dopa uptake.

With regard to the issue of whether ^{18}F-dopa uptake is a valid measure of PD progression, there is evidence from both human post-mortem studies (Snow, 1993) and MPTP-lesioned monkeys (Pate, 1993) that striatal Ki^{o} values correlate with both nigral cell counts and dopaminergic terminal dopamine and tyrosine hydroxylase levels. Although it could be argued that PD is not only about dopamine and that ^{18}F-dopa PET is assessing only one aspect of the condition, cross-sectional studies have shown that putamen Ki^{o} values correlate closely with both bradykinesia and rigidity in individual patients with PD (Otsuka, 1996).

Study results

This study attempted to establish whether dopamine agonists have a disease-modifying or neuroprotective effect as judged by comparing the rate of loss of dopamine terminal function between ropinirole and L-dopa PD cohorts with ^{18}F-dopa PET. The number of PD patients recruited into this single PET centre study was relatively small ($n = 45$). Furthermore, at the start of the study (1994), the sensitivity and variability of the technique in following disease progression had not been established. Therefore, it was not at that time possible to calculate the number of PD patients required to provide 80% power to demonstrate, for example, a 25% difference between ITT treatment groups ($p < 0.05$). Data from our study suggests that 80 patients in each cohort would be required. The numbers in our study were only sufficient to demonstrate a 50% disease-modifying effect and so smaller differences in the rate of progression between ropinirole and levodopa cohorts would not achieve significance.

Another important factor in our study factor was the 2:1 randomisation. This was employed because patients were studied parallel to a clinical study with the same randomisation (Rascol, 2000) but after patient withdrawals, this resulted in a small number of patients in the L-dopa arm of our study. Interestingly, however, another ^{18}F-dopa PET study on recent onset PD progression (mean symptom duration 18.3 ± 6.5 months; $n = 10$) (Morrish, 1996) reported a similar annual decline in putamen Ki^{o} (12.3% versus 9% in our study), in levodopa treated PD patients.

Over the course of the first two years of the trial, patients showed a significantly greater increase in clinical disability in the ITT ropinirole arm compared with the ITT L-dopa arm (11 versus 8 points when "off" on the UPDRS motor subscale). The problem, however, in interpreting these clinical observations is that L-dopa is known to be a more effective symptomatic agent than ropinirole in PD patients with established disease (Hoehn and Yahr stage III). Therefore, one cannot discriminate from clinical data alone, relative symptomatic from potentially neuroprotective effects of drug treatment. This problem arose in the DATATOP study (Deprenyl and Tocopherol Antioxidative Therapy of Parkinsonism: Parkinson Study Group, 1989, 1993), when it was initially thought that selegiline (deprenyl) had demonstrated a neuro-protective effect in early PD but when on further analysis, it was considered to be primarily a symptomatic effect (Schulzer, 1992).

When symptom duration was taken into account, patients taking ropinirole ($n = 17$) with symptomatic disease duration of <2 years showed a 14% mean reduction in putamen Ki^o compared with a 28% reduction in the corresponding L-dopa group ($n = 4$) ($p = 0.15$) over the two year period. Clearly, because of the very small numbers in the L-dopa subgroup, this observation should be treated with caution and was not, therefore, presented in the results section. Nevertheless, this trend is potentially interesting and as a consequence, a further appropriately powered, double-blind, randomised (1:1), international multi-centre PET study ($n = 160$) is currently being undertaken to evaluate this further.

Conclusion

In summary, our study suggests that overall after two years treatment in subjects with early PD, there is no significant difference in the rate of progression between patients started on ropinirole compared with L-dopa therapy. We have also demonstrated the ^{18}F-dopa PET can be used to evaluate the efficacy of novel neuroprotective or disease modifying agents.

Acknowledgements

We would like to thank Prof. O. Rascol, Toulouse, France for recruiting patients, the chemists, N. Steel and M. Constantinou for producing ^{18}F-dopa, the radiographers, D. Griffiths, H. McDevitt and A. Blyth for assisting in scanning. J.S.R. was supported by an educational grant from SmithKline Beecham U.K.

References

Alexander T, Sortwell CE, Sladek CD, Roth RH, Steece-Collier K (1997) Comparison of neurotoxicity following repeated administration of L-dopa, D-dopa, and dopamine to embryonic mesencephalic dopamine neurons in cultures derived from Fischer 344 and Sprague-Dawley donors. Cell Transplant 6: 309–315

Asanuma M, Ogawa N, Nishibayashi S, Kawai M, Kondo Y, Iwata E (1995) Protective effects of pergolide on dopamine levels in the 6-hydroxydopamine-lesioned mouse brain. Arch Int Pharmacodyn 329: 221–230

Badawi RD (1997) 3D-mode acquisition in clinical PET. Nucl Med Commun 18: 801–804

Bailey DL (1992) 3D acquisition and reconstruction in positron emission tomography. Ann Nucl Med 6: 123–130

Bailey DL, Meikle SR (1994) A convolution-subtraction scatter correction method for 3D PET. Phys Med Biol 39: 411–424

Brooks DJ, Salmon EP, Mathias CJ, et al (1990) The relationship between locomotor disability, autonomic dysfunction, and the integrity of the striatal dopaminergic system in patients with multiple system atrophy, pure autonomic failure, and Parkinson's disease, studied with PET. Brain 113: 1539–1552

Brooks DJ, Ibanez V, Sawle GV, et al (1990) Differing patterns of striatal ^{18}F-Dopa uptake in Parkinson's disease, multiple system atrophy, and progressive supranuclear palsy. Ann Neurol 28: 547–555

Eden RJ, Costall B, Domeney AM, et al (1991) Preclinical pharmacology of ropinirole (SK&F 101468-A), a novel dopamine agonist. Pharmacol Biochem Behav 38: 147–154

Fahn S, Elton RL, Members of the UPDRS Development Committee (1987) Unified Parkinson's Disease Rating Scale. In: Fahn S, Marsden CD, Calne DB, Goldstein M (eds) Recent developments in Parkinson's disease. MacMillan Healthcare Information, Florham Park (NJ), pp 153–163

Fears R, Bowen WP, Eden RJ, Kay S (1994) Neurochemical selectivity and D_3 affinity of the novel dopaminergic agonist ropinirole. New Trends Clin Neuropharmacol 8: 298

Felten DL, Felten SY, Fuller RW, et al (1992) Chronic dietary pergolide preserves nigrostriatal neuronal integrity in aged Fischer 344 rats. Neurobiol Aging 13: 339–351

Garnett ES, Firnau G, Nahmias C (1983) Dopamine visualized in the basal ganglia of living man. Nature 305: 137–138

Gassen M, Gross A, Youdim MBH (1996) Apomorphine is a highly potent free radical scavenger in rat brain mitochondrial fraction. Eur J Pharmacol 308: 219–225

Gibb WRG, Lees AJ (1988) The relevance of the Lewy body to the pathogenesis of idiopathic Parkinson's disease. J Neurol Neurosurg Psychiatry 51: 745–752

Graham DJ, Tiffany SM, Bell WR, Gutknecht WF (1978) Auto-oxidation versus covalent binding of quinones as the mechanism of toxicity of dopamine, 6-hydroxydopamine and related compounds towards C1300 neuroblastoma cells in vitro. Mol Pharmacol 14: 644–653

Hoehn MM, Yahr MD (1967) Parkinsonism: onset, progression and mortality. Neurology 17: 427–442

Iida M, Miyazaki I, Tanaka K, Kabuto H, Iwata-Ichikawa E, Ogawa N (1999) Dopamine D2 receptor-mediated antioxidant and neuroprotective effects of ropinirole, a dopamine agonist. Brain Res 838: 51–59

Ishikawa T, Dhawan V, Chaly T, et al (1996) Fluorodopa positron emission tomography with an inhibitor of catechol-O-methyltransferase: effect of the plasma 3-O-methyldopa fraction on data analysis. J Cereb Blood Flow Metab 16: 854–863

Kish SJ, Shannak K, Hornykiewicz O (1988) Uneven pattern of dopamine loss in the striatum of patients with idiopathic Parkinson's disease. N Engl J Med 318: 876–880

Martin WRW, Palmer MR, Patlak CS, Calne DB (1989) Nigro-striatal function in man studied with positron emission tomography. Ann Neurol 26: 535–542

Mena MA, Pardo B, Casarejos MJ, Fahn S, de Yebenes JG (1992) Neurotoxicity of L-dopa on catecholamine-rich neurons. Mov Disord 7: 23–31

Mena MA, Pardo B, Paino CL, de Yebenes JG (1993) L-dopa toxicity in fetal rat midbrain neurons in culture: modulation by ascorbic acid. Neuroreport 4: 438–440

Michel PP, Hefti F (1990) Toxicity of 6-hydroxydopamine and dopamine for dopaminergic neurons in culture. J Neurosci Res 26: 428–435

Morrish PK, Sawle GV, Brooks DJ (1996) An [^{18}F]dopa-PET and clinical study of the rate of progression in Parkinson's disease. Brain 119: 585–591

Morrish PK, Rakshi JS, Brooks DJ (1997) Can the neuroprotective efficacy of an agent ever be conclusively proven? Eur J Neurol 4 [Suppl 3]: S19–24

Morrish PK, Rakshi JS, Sawle GV, Brooks DJ (1998) Measuring the rate of progression and estimating the preclinical period of Parkinson's disease with [^{18}F]dopa PET. J Neurol Neurosurg Psychiatry 64: 314–319

Newcomer TA, Rosenberg PA, Aizenman E (1995) Iron-mediated oxidation of 3,4-dihydroxyphenylalanine to an excitotoxin. J Neurochem 64: 1742–1748

Ogawa N, Tanaka K, Asanuma M, et al (1994) Bromocriptine protects mice against 6-hydroxydopamine and scavenges hydroxyl free radicals in vitro. Brain Res 657: 207–213

Olanow CW, Calne D (1991) Does selegiline monotherapy in Parkinson's disease act by symptomatic or protective mechanism? Neurol 321: 1364–1371

Otsuka M, Ichiya Y, Kuwabara Y, et al (1996) Differences in the reduced ^{18}F-Dopa uptakes of the caudate and the putamen in Parkinson's disease: correlations with the three main symptoms. J Neurol Sci 136: 169–173

Parkinson Study Group (1989) Effect of selegiline (deprenyl) on the progression of disability in early Parkinson's disease. N Engl J Med 321: 1364–1371

Parkinson Study Group (1993) Effects of tocopherol and deprenyl on the progression of disability in early Parkinson's disease. N Engl J Med 328: 176–183

Pate BD, Kawamata T, Yamada T, et al (1993) Correlation of striatal fluorodopa uptake in the MPTP monkey with dopaminergic indices. Ann Neurol 34: 331–338

Rakshi JS, Bailey DL, Morrish PK, Brooks DJ (1996) Implementation of 3D acquisition, reconstruction and analysis of dynamic fluorodopa studies. In: Myers R, Cunningham V, Bailey DL, Jones T (eds) Quantification of brain function using PET. Academic Press, San Diego, pp 82–87

Rakshi JS, Uema T, Ito K, et al (1999) Frontal, midbrain and striatal dopaminergic function in early and advanced Parkinson's disease: a 3D [^{18}F]dopa-PET study. Brain 122: 1637–1650

Rascol O, Brooks DJ, Korczyn AD, De Deyn P, Clarke C, Lang AE (2000) Dyskinesia in Parkinson's disease: a 5-year study of ropinirole versus levodopa. N Engl J Med 342: 1484–1491

Sawle GV, Burn DJ, Morrish PK, et al (1994) The effect of entacapone (OR-611) on brain [18F]-6-L-fluorodopa metabolism: implications for levodopa therapy of Parkinson's disease. Neurology 44: 1292–1297

Schulzer M, Mak E, Calne DB (1992) The antiparkinsonian efficacy of deprenyl derives from transient improvement that is likely to be symptomatic. Ann Neurol 32: 795–798

Snow BJ, Tooyama I, McGeer EG, et al (1993) Human positron emission tomographic [18F]fluorodopa studies correlate with dopamine cell counts and levels. Ann Neurol 34: 324–330

Tanaka M, Sotomatsu A, Kanai H, Hirai S (1991) Dopa and dopamine cause cultured neuronal death in the presence of iron. J Neurol Sci 101: 198–203

Talairach J, Tournoux P (1988) Co-planar stereotaxic atlas of the human brain. G Thieme, Stuttgart

Trebossen R, Bendriem B, Fontaine A, Frouin V, Remy P (1996) Quantification of the [^{18}F] fluorodopa uptake in the human striata in 3D PET with the ETM scatter correction. In: Myers R, Cunningham V, Bailey DL, Jones T (eds) Quantification of brain function using PET. Academic Press, San Diego, pp 88–92

Turjanski N, Lees AJ, Brooks DJ (1999) Striatal dopaminergic receptor dysfunction in patients with restless legs syndrome: ^{18}F-dopa and ^{11}C-raclopride PET studies. Neurology 52: 932–937

Vingerhoets FJG, Snow BJ, Schulzer M, et al (1996). Reproducibility and discriminating ability of fluorine-18-6-fluoro-L-dopa PET in Parkinson's disease. J Nucl Med 37: 421–426

Weinhard K (1998) 3D [18F]dopa-PET: improved kinetics and discrimination in Parkinson's disease. In: Bendriem B, Townsend DW (eds) The theory and practice of 3D PET. Kluwer Academic Publishers, Dordrecht, pp 150–154

Authors' address: J. S. Rakshi, MRCP, Specialist Registrar, National Hospital for Neurology and Neurosurgery, Queen Square, London WC1N 3BG, United Kingdom

TECHNICAL NOTE

Radiation Medicine: Vol. 21 No. 1, 47–54 p.p., 2003

New Insight into the Analysis of 6-[^{18}F]fluoro-L-DOPA PET Dynamic Data in Brain Tissue without an Irreversible Compartment: Comparative Study of the Patlak and Logan Analyses

Shoji Kawatsu,* Takashi Kato,* Atsuko Nagano-Saito, Kentaro Hatano,* Kengo Ito,* and Takeo Ishigaki*****

The objective of this study was to show that the Logan analysis is theoretically more appropriate than the Patlak analysis for the assessment of 6-[^{18}F] fluoro-L-DOPA (FDOPA) positron emission tomography (PET) dynamic data in brain tissue without an irreversible compartment, e.g., occipital cortex. Another purpose was to provide the first application of this analysis to real data. Ten normal controls (NC), 10 Parkinson's disease (PD) patients, and 10 Parkinson's disease with dementia (PDD) patients underwent FDOPA PET. The Logan analysis and the Patlak analysis were applied to the occipital cortex with the cerebellum as a reference tissue. In the occipital cortex, the Logan analysis showed a significant difference ($p=0.018$) between NC and PDD patients. However, the Patlak analysis showed no significant differences, but larger variances. The Logan analysis of FDOPA PET dynamic data in the occipital cortex was considered to be theoretically appropriate and to provide new insight into the analysis of that region.

Key words: FDOPA, PET, Logan analysis, Patlak analysis

Introduction

6-[^{18}F] fluoro-L-dopa (FDOPA) positron emission tomography (PET) has been successfully used to evaluate presynaptic striatal dopaminergic function in humans. In the striatum, it is widely accepted that the rate of influx of the tracer from plasma into the irreversible compartment of brain tissue calculated from the Patlak analysis is effective for discriminating between normal controls (NC) and Parkinson's disease (PD) patients.[1,2] Recently, FDOPA PET was used to estimate the influx rate of FDOPA into extrastriatal regions, as well as into the striatum. The Patlak analysis was used with the cerebellum or occipital cortex as reference tissues.[3-5] However, whether or not the Patlak analysis provides reliable quantification in extrastriatal regions is an open question. The Patlak analysis assumes an irreversible compartment.[6,7] Nevertheless, for the kinetics of FDOPA, the extrastriatal region has either a negligible or non-existent number of irreversible compartments since the influx rates of FDOPA were reported as low or nil.[1,8,9] Thus, in extrastriatal regions, the Patlak analysis may be inadequate to discriminate subtle differences between NC and PD patients. On the other hand, a recent study reports that the occipital cortex shows significant differences in the metabolic measurements of PD patients[10] and dementia-with-Lewy-bodies (DLB) patients.[11-14] However, previous FDOPA PET studies using the Patlak analysis reported no significant differences in the occipital cortex among NC, PD patients, and Parkinson's disease with dementia (PDD) patients, where PDD and DLB have been considered to intersect.[15] The occipital cortex is considered to have no irreversible compartments with respect to the kinetics of FDOPA. Therefore, the Patlak analysis may be theoretically inadequate for analysis of

Received August 27, 2002; revision accepted November 28, 2002.

*Department of Biofunctional Reserch, National Institute for Longevity Sciences

**Department of Neurology, Chubu National Hospital

***Department of Radiology, Nagoya University School of Medicine

Reprint requests to Shoji Kawatsu, M.D., Department of Biofunctional Research, National Institute for Longevity Sciences 36-3, Gengo, Morioka-cho, Obu, Aichi 474-8522, JAPAN.

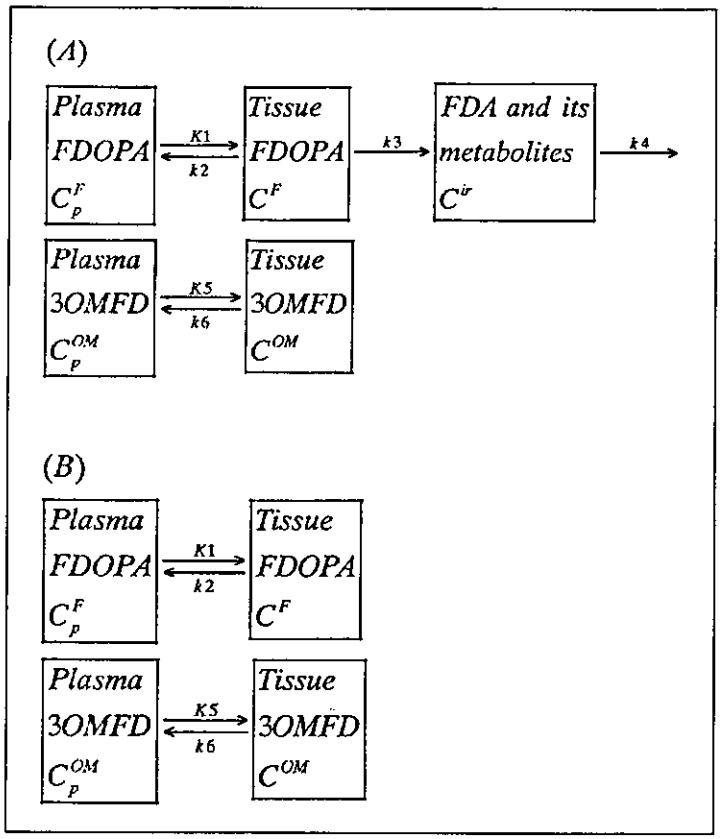

Fig. 1.
A: FDOPA and 3OMFD compartment models with irreversible compartments denoted as follows; K1 and K5 (mL g^{-1} min^{-1}) as the rate constants that represent the BBB transport of FDOPA and 3OMFD, respectively; k2 and k6 (min^{-1}) as the reverse BBB transport rate constants of FDOPA and 3OMFD, respectively; k3 (min^{-1}) as the rate constant from the tissue FDOPA compartment to the combined compartment of FDA and its metabolites; k4 (min^{-1}) as the clearance rate constant of 18F from the compartment of FDA and its metabolites to plasma. $C_p^F(t)$ and $C_p^{OM}(t)$ denote the concentrations of FDOPA and 3OMFD in plasma, respectively. $C^F(t)$ and $C^{OM}(t)$ denote those in plasma, respectively. $C^{ir}(t)$ denotes the concentration of the tracer in an irreversible compartment. B: FDOPA and 3OMFD compartment models without an irreversible compartment.

the occipital cortex and has failed to detect subtle differences between groups. Moreover, the Patlak analysis of FDOPA was found to be markedly biased before 120 min. A key hypothesis of the Patlak analysis is that reversible compartment radioactivity is in effective equilibrium with the tracer in plasma.[6,7] This is violated before 120 min.[16] Therefore, when the scan time is less than 120 min, the Patlak analysis may again be inadequate to discriminate subtle differences between groups. As a result, when the target region has no irreversible compartment, e.g., occipital cortex or cerebellum, and the scan time is less than 120 min, other analyses must be considered for FDOPA PET dynamic data.

In this article, we describe theoretical considerations for FDOPA PET analysis in regions without an irreversible compartment and present an adequate analysis. We then provide the first application of this analysis using real data.

Theory

The compartmental model for FDOPA and 3-O-methyl-6-[^{18}F]fluoro-L-DOPA (3OMFD)[17] is shown in Fig. 1, using the following rate constants: K1 and K5 (mL g^{-1} min^{-1}) as the rate constants that represent the blood brain barrier (BBB) transport of FDOPA and 3OMFD, respectively; k2 and k6 (min^{-1}) as the reverse BBB transport rate constants of FDOPA and 3OMFD, respectively; k3 (min^{-1}) as the rate constant from the tissue FDOPA compartment to the combined compartment of 6-[^{18}F]fluorodopamine (FDA) and its metabolites; and k4 (min^{-1}) as the clearance rate constant of ^{18}F from the compartment of FDA and its metabolites to plasma. The suffixes Oc and Ce denote the rate constants for the occipital cortex and cerebellum, respectively. Three conditions were assumed regarding the values of the rate constants.

1. The transport rate constants of 3OMFD relative to FDOPA were constrained to unity, i.e., K1/K5=1.[1]

2. The distribution volumes of FDOPA and 3OMFD in the cerebellum and occipital cortex were assumed to have the same values, i.e., K1/k2=K5/k6.[18]

3. The rate constant k4 was assumed to be zero.[1,18]

For the two-compartment model of FDOPA and 3OMFD,

$$\frac{dC_{Oc}^F(t)}{dt} = K1_{Oc}C_P^F(t) - k2_{Oc}C_{Oc}^F(t) \quad (1)$$

$$\frac{dC_{Oc}^{OM}(t)}{dt} = K5_{Oc}C_P^{OM}(t) - k6_{Oc}C_{Oc}^{OM}(t) \quad (2)$$

where $C_{Oc}^{F}(t)$ and $C_{Oc}^{OM}(t)$ denote the concentrations of FDOPA and 3OMFD in occipital cortex, respectively. $C_P^{F}(t)$ and $C_P^{OM}(t)$ denote those in plasma, respectively. Following the above constraints for the rate constants, it is easy to see that $K1_{Oc}=K5_{Oc}$, and $k2_{Oc}=k6_{Oc}$. It follows from equations (Eqs.) 1 and 2 that

$$\frac{dC_{Oc}(t)}{dt} = K1_{Oc}C_P(t) - k2_{Oc}C_{Oc}(t) \quad (3)$$

where $C_{Oc}(t) = C_{Oc}^{F}(t) + C_{Oc}^{OM}(t)$, and $C_P(t) = C_P^{F}(t) + C_P^{OM}(t)$. Since the cerebellum is assumed under the same kinetic model as the occipital cortex, the same type equation

$$\frac{dC_{Ce}(t)}{dt} = K1_{Ce}C_P(t) - k2_{Ce}C_{Ce}(t) \quad (4)$$

holds for the cerebellum. Integrating Eqs. 3 and 4 with respect to time variable t and eliminating the integrated term $C_P(t)$, we have the equation,

$$\frac{\int_0^t C_{Oc}(u)dux}{C_{Oc}(t)} = DVR\frac{\int_0^t C_{Ce}(u)du}{C_{Oc}(t)} - \frac{1}{k2_{Oc}} \cdot + DVR\frac{C_{Ce}(t)}{C_{Oc}(t)}\frac{1}{k2_{Ce}} \quad (5)$$

where $DVR=(K1_{Oc}/k2_{Oc})/(K1_{Ce}/k2_{Ce})$ is the distribution volume ratio of the occipital cortex to cerebellum.

The last term on the right-hand side of Eq. 5 varies with time. Logan introduced the population mean of the rate constant, i.e., $\overline{k2_{Ce}}$ and translated Eq. 5 into the equation of the Logan plot.[19]

$$\frac{\int_0^t C_{Oc}(u)du}{C_{Oc}(t)} = DVR\left[\frac{\int_0^t C_{Ce}(u)du + \frac{C_{Ce}(t)}{\overline{k2_{Ce}}}}{C_{Oc}(t)}\right] - \frac{1}{k2_{Oc}} + DVR\frac{C_{Ce}(t)}{C_{Oc}(t)}\left(\frac{1}{k2_{Ce}} - \frac{1}{\overline{k2_{Ce}}}\right) \quad (6)$$

The value $\overline{k2_{Ce}}$=0.057 (min^{-1}) was used in this study.[16,17] The last term on the right-hand side of Eq. 6 is a small error term.[19] Thus the intercept of the Logan plot depends almost entirely on $-1/k2_{Oc}$. In Eq. 6 of the Logan plot, the radioactivity from tissue plasma volume is not included, since the blood volume of about 5% was neglected for simplicity.[17]

According to the Patlak analysis,

$$\frac{dC_{Oc}(t)}{dt} = K1_{Oc}C_P(t) - (k2_{Oc} + k3_{Oc})C_{Oc}(t) \quad (7)$$

$$\frac{dC_{Oc}^{ir}(t)}{dt} = k3_{Oc}C_{Oc}(t) \quad (8)$$

$$\frac{dC_{Ce}(t)}{dt} = K1_{Ce}C_p(t) - k2_{Ce}C_{Ce}(t) \quad (9)$$

where $C_{Oc}^{ir}(t)$ denotes the concentration of tracer in an irreversible compartment. The formula is applicable even if the rate constant $k3_{Oc}$ is zero. From Eqs. 7, 8, and 9, Eq. 10 follows:

$$\frac{C_{Oc}(t)+C_{Oc}^{ir}(t)}{C_{Ce}(t)} = \frac{k2_{Ce}}{K1_{Ce}}\frac{K1_{Oc}k3_{Oc}}{k2_{Oc}+k3_{Oc}}\frac{\int_0^t C_{Ce}(u)du}{C_{Ce}(t)} + \frac{1}{K1_{Ce}}\frac{K1_{Oc}k3_{Oc}}{k2_{Oc}+k3_{Oc}} + \frac{k2_{Oc}}{k2_{Oc}+k3_{Oc}}\frac{C_{Oc}(t)}{C_{Ce}(t)} \quad (10)$$

If Patlak's condition of effective equilibrium, i.e., $C_{Oc}(t)=[K1_{Oc}/(k2_{Oc}+k3_{Oc})]C_P(t)$ and $C_{Ce}(t)=(K1_{Ce}/k2_{Ce})C_P(t)$,[6,7] holds at later times, then the well-known equation of the Patlak plot

$$\frac{C_{Oc}(t)+C_{Oc}^{ir}(t)}{C_{Ce}(t)} = \frac{k2_{Ce}}{K1_{Ce}}\frac{K1_{Oc}k3_{Oc}}{k2_{Oc}+k3_{Oc}}\frac{\int_0^t C_{Ce}(u)du}{C_{Ce}(t)} + \frac{1}{K1_{Ce}}\frac{K1_{Oc}k3_{Oc}}{k2_{Oc}+k3_{Oc}} + \frac{k2_{Ce}}{K1_{Ce}}\frac{K1_{Oc}k2_{Oc}}{(k2_{Oc}+k3_{Oc})^2} \quad (11)$$

follows. If $k3_{Oc}$ is zero Eq. 11 becomes

$$\frac{C_{Oc}(t)}{C_{Ce}(t)} = \frac{K1_{Oc}}{k2_{Oc}}\Big/\frac{K1_{Ce}}{k2_{Ce}} \quad (12)$$

However, the condition of effective equilibrium is violated before 120 min, and the linear asymptotic property of the Patlak plot may be violated before 120 min.[16] Therefore Eq. 12 may not hold. On the other hand, the condition of effective equilibrium was not used in the derivation of Eq. 6 of the Logan plot. Therefore, Eq. 6 holds even if the condition of effective equilibrium is violated. In Eq. 6 of the Logan plot, the last term on the right-hand side of the equation varies with time. However, by introducing $\overline{k2_{Ce}}$, variance is decreased. Thus, the variance with time of the Logan plot is much smaller than that of the Patlak plot. This makes the Logan plot more practical.

Methods

Ten patients with idiopathic PD without dementia [age, 65.8±6.7 (mean ± standard deviation (SD)) years] and 10 patients with PDD (age, 67.1±6.5 years) were recruited from the Chubu National Hospital Neurology Clinic. All PD patients fulfilled the United Kingdom

Brain Bank criteria for diagnosis of this disorder. The PDD patients met the criteria for PDD, namely Parkinsonism plus dementia, where motor manifestations preceded the cognitive symptoms by at least one year.[15] Although PDD patients included some cases with relatively high Mini-Mental State Examination (MMSE) scores, all fulfilled the Diagnostic and Statistical Manual of Mental Disorders Fourth Edition (DSM IV) criteria for dementia. Each patient was assessed clinically by a neurologist before PET and at least 48 hours after discontinuing medications. The PDD patients in this study were given no specific treatment for their dementia, such as acetylcholinesterase inhibitors. A separate group of 10 NCs (age 67.6±5.1 years) was recruited, and subjects were scanned over the same time period. Neurologists at Chubu National Hospital confirmed that they did not have any neurological disorders. NCs displayed no significant abnormalities except for normal age-related changes such as dilated perivascular spaces on magnetic resonance (MR) images. Permission to perform these studies was obtained from the Ethics Committee of National Chubu Hospital. All of the subjects gave written informed consent prior to PET scanning.

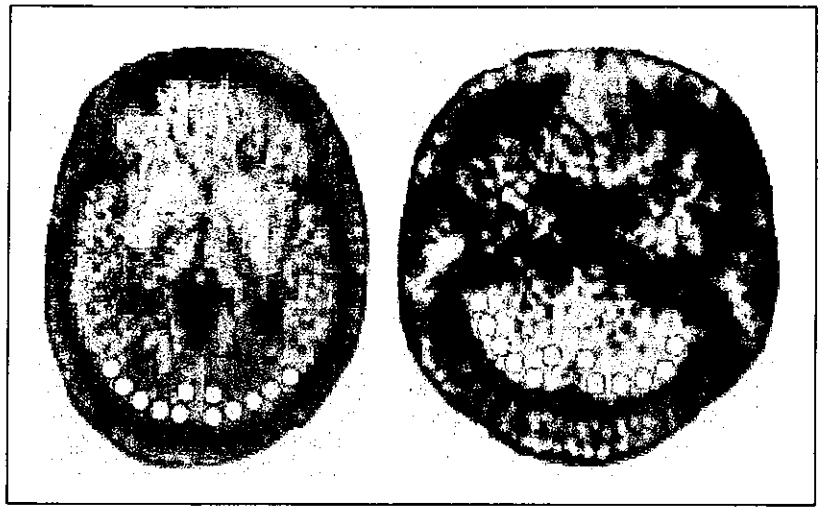

Fig. 2.
A: Slice showing an example of cerebellar cortex ROIs. B: Slice showing an example of occipital cortex ROIs. White filled circles denote ROIs.

All subjects were given 100 mg of oral carbidopa 1 hour before scanning. Dynamic FDOPA-PET studies were performed using an ECAT EXACT HR47 (CTI/ Siemens, Knoxville, TN) in three-dimensional acquisition mode. This yielded 47 simultaneous planes with an axial full-width half-maximum resolution of 4.8 mm and an in-plane resolution of 3.9×3.9 mm. The correction for tissue attenuation of 511 keV γ-radiation was measured using a retractable 68Ga/68Ge source.

FDOPA (80-180 MBq) in normal saline solution was infused intravenously over 30 seconds. Scanning began at the start of tracer injection. The protocol included 25 time frames (4×1 min, 3×2 min, 3×3 min, 15×5min) over 94 min.

Image data analysis was performed on a Sun workstation (Sun Microsystems, Silicon Valley, CA), and successive statistical data analysis was performed on a PC using SPSS Version 10 (SPSS Inc, Chicago, IL, 1998). To correct for head movements between scans, images from each subject were aligned using the alignment program in SPM95 (Welcome Department of Cognitive Neurology, London). After corrections for head movements and radioactivity decay, the integrated 'add image' (0-94) was obtained from all the time frames of the subject. Regions of interest (ROIs) were manually determined from the 'add image', which covered most of the cerebellum and occipital cortex, respectively. Examples of ROIs are shown in Fig. 2. The cerebellar ROIs contained five to seven slices. The occipital ROIs contained 7 to 10 slices. The ROIs were used for all time frames of the subject. The mean values of the ROIs were used for graphical analysis. The Logan analysis using Eq. 6, and the Patlak analysis using Eq. 13 were performed with the cerebellum as reference tissue. Linear regression was performed for data frames 12-25. As mentioned in the theory section, the slope and intercept of the Logan plot represent FDOPA DVR and $-1/k2_{oc}$. Those of the Patlak plot represent the FDOPA influx constant and DVR. Dunnett's multiple comparisons test was used to test for statistically significant differences in the values of intercepts and slopes that resulted from the Logan and Patlak analyses among the three groups (i.e., NC, PD, and PDD). P values <0.05 were considered to be statistically significant.

RESULTS

The results shown in Fig. 3 are examples of tissue time-activity curves (filled squares, cerebellar cortex; filled circles, occipital cortex) for NC-(A), PD-(B), and PDD-(C), respectively, after an intravenous bolus injection of FDOPA. The results shown in Fig. 4 are examples of the Logan plot (squares, plot; line, linear regression for data frames 12-25) for NC-(A), PD-(B), and PDD-(C), respectively. Data were taken from the same subjects as

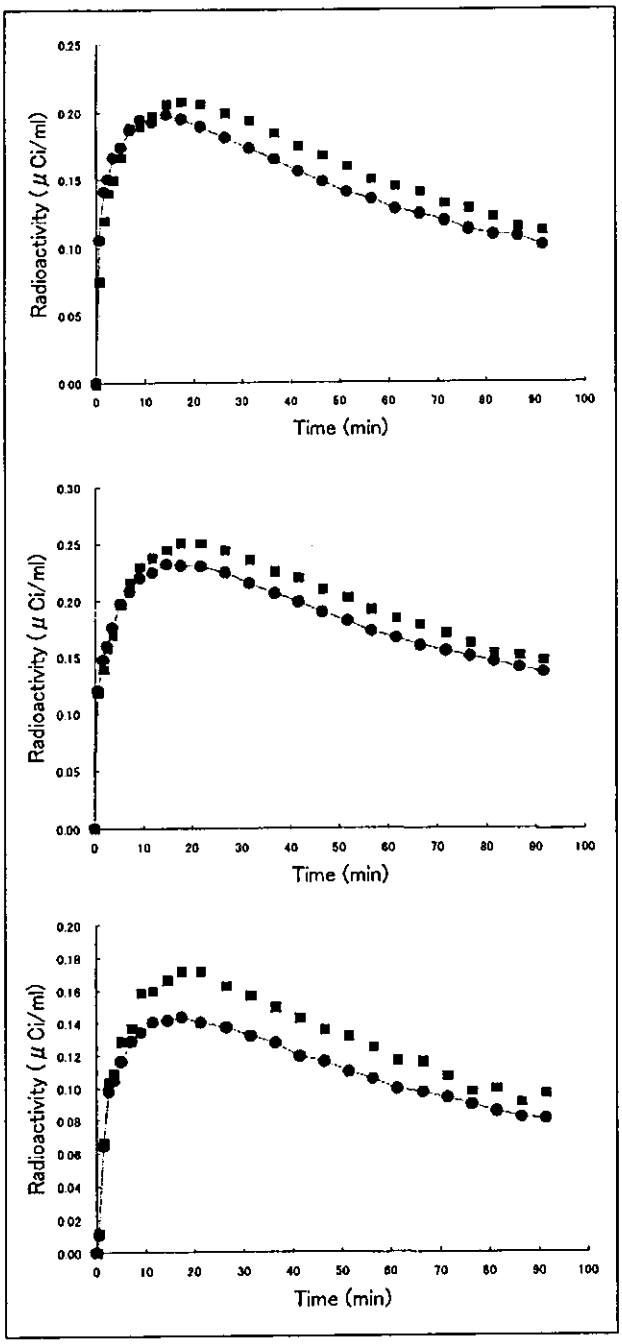

Fig. 3.
A, B, and C are examples of tissue time-activity curves (filled squares, cerebellar cortex; filled circles, occipital cortex) for NC, PD, and PDD, respectively, after an intravenous bolus injection of FDOPA.

A
B
C

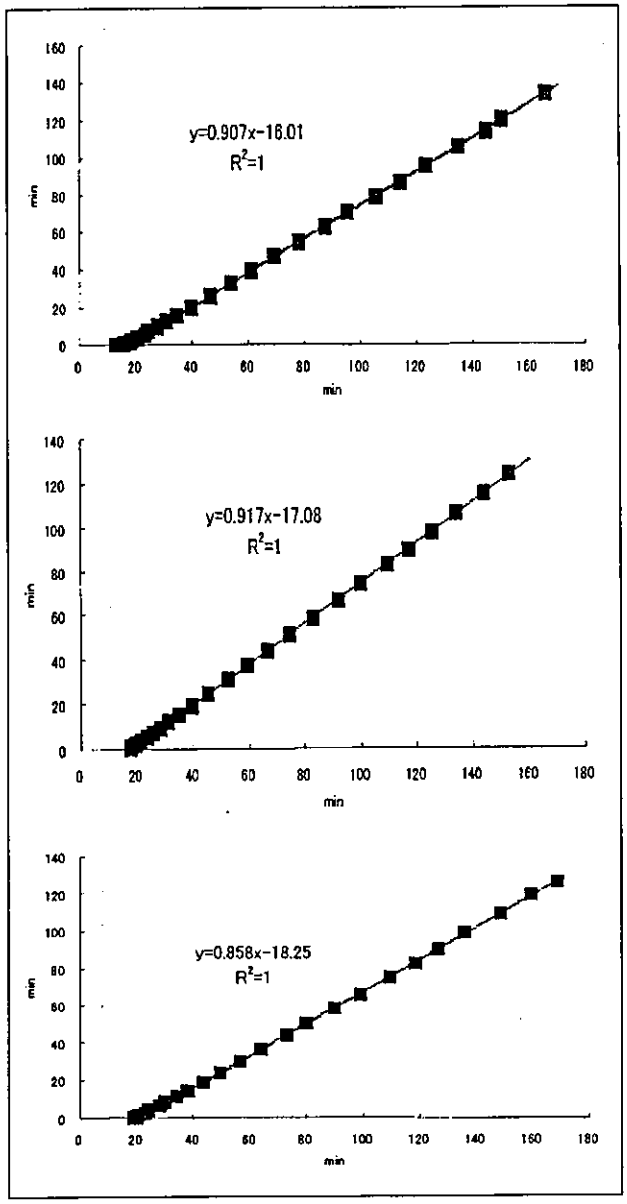

Fig. 4.
A, B, and C are examples of the Logan plot (squares, plot; line, linear regression for data frames 12-25) for NC, PD, and PDD, respectively. Plots were taken from the same subjects shown in Fig. 3. R^2s are coefficients of determination of the linear regression. The Logan plot showed good linear regression.

A
B
C

in Fig. 3. The Logan plot showed good linear regression. R^2s are coefficients of determination of the linear regression. The results shown in Fig. 5 are examples of the Patlak plot (squares, plot; line, linear regression for data frames 12-25) for NC-(A), PD-(B), and PDD-(C), respectively. Data were taken from the same subjects as in Fig. 3. The Patlak plot showed poor linear regression. The results shown in Table 1 are the means ± SDs of fitting results of the slope and intercept of the Logan plot for the three groups. The SDs were all within 10% of the mean values within each group. The means of the intercepts of PD and PDD were lower than that of NC (Table 1). The coefficients of determination of the linear regression of the Logan plot all equaled 1.00; thus the

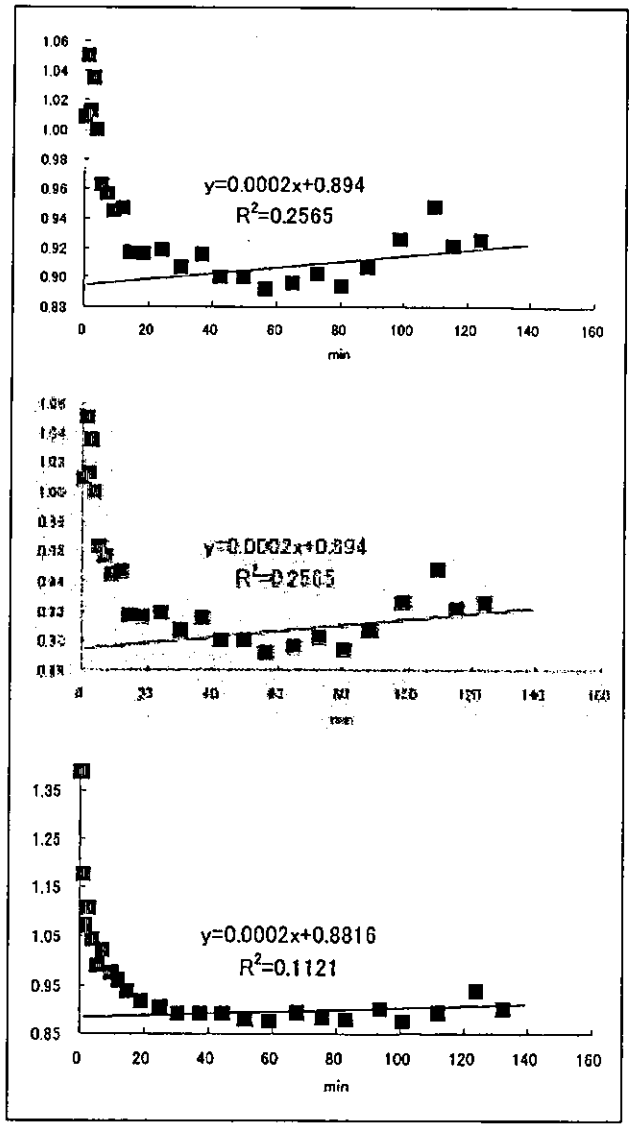

Fig. 5.
A, B, and C are examples of Patlak plots (squares, plot; line, linear regression for data frames 12-25) for NC, PD, and PDD, respectively. Plots were taken from the same subjects shown in Fig. 3. R^2s are coefficients of determination of the linear regression. The Patlak plot showed low coefficients of determination and poor linear regression.

A

B

C

Logan plot showed good linear regression. When Dunnett's multiple comparisons test was used for the results of the intercept of the Logan plot using NC as a reference, significant differences were shown only between NC and PDD (p=0.018). No significant differences were detected for the results of the slope of the Logan plot.

The results shown in Table 2 are the means ± SDs of fitting results of the slope and intercept of the Patlak plot for the groups. When Dunnett's multiple comparisons

Table 1. Results of the Logan plot of FDOPA PET in the occipital cortex

	Slope Mean±SD	Intercept (min) Mean±SD
NC	0.89±0.05	−16.54±1.16
PD	0.87±0.07	−17.84±1.57
PDD	0.89±0.09	−18.19±1.20

Table 2. Results of the Patlak plot of FDOPA PET in the occipital cortex

	Slope (min^{-1}) Mean±SD	Intercept Mean±SD
NC	0.000113±0.000258	0.877±0.0615
PD	0.000366±0.000259	0.840±0.0628
PDD	0.000364±0.000238	0.862±0.0825

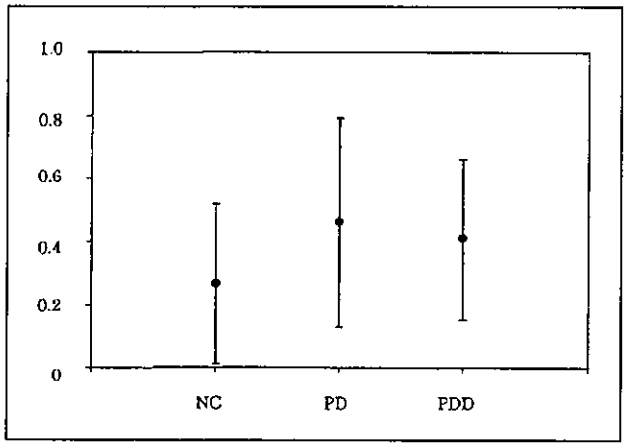

Fig. 6.
Distribution of the coefficients of determination of the linear regression of the Patlak plot of FDOPA PET are shown. Filled circles denote mean values. Error bars denote SD.

test was used for the results of the intercept of the Patlak plot using the NC as a reference, no significant differences were shown. The coefficients of determination of the linear regression are shown in Figs. 4, 5, and 6. The coefficients of determination of the Patlak plot showed low values in many cases (Figs. 5 and 6).

Discussion

Recently, FDOPA PET has been used to estimate the rate of influx of FDOPA in extrastriatal regions and the striatum with the use of the Patlak analysis and with the cerebellum or occipital cortex as reference tissues.[3-5]

However, the reliability of the Patlak analysis of FDOPA PET in extrastriatal regions has not been studied in detail. Moreover, according to the protocol, scan times are less than 120 min, while the Patlak analysis of FDOPA is markedly biased before 120 min.[16] In the present study, we analyzed the occipital cortex since an alternative graphical analysis, i.e., the Logan analysis, was found to be appropriate. Since the kinetics of FDOPA are more complicated, dynamic studies with blood sampling will be required for other extrastriatal regions to clarify the reliability of the Patlak analysis of FDOPA PET.

The present FDOPA PET study with a scan time of 94 min showed that the Patlak analysis was unstable in the occipital cortex, with the cerebellum as reference tissue. Therefore, the Patlak analysis, with the cerebellum as reference tissue, may be inadequate in the occipital cortex. In extrastriatal regions, results from the Patlak analysis of FDOPA PET should be interpreted with careful consideration.

Cerebellum and occipital cortex are considered to have no irreversible compartments with respect to the kinetics of FDOPA. In these regions, the Logan analysis is a good choice for graphical analysis, since it assumes that no irreversible compartments are present in the ROI.[19,20] Moreover, the Logan analysis is stable even for the short times of dynamic scans.[19] Thus, the Logan analysis may have the power to provide reliable quantification for FDOPA time-course data within 94 min. The present results showed that the Logan analysis in the occipital cortex was stable and showed significant differences between NC and PDD patients. However, the Patlak analysis in the occipital cortex showed large variances and indicated no significant differences among the three groups. Nonetheless, it is widely accepted that the Patlak analysis in the striatum has the power to discriminate between NC and PD. Therefore, the Logan analysis in the occipital cortex with the Patlak analysis in the striatum make it possible to discriminate among NC, PD, and PDD when comparing these groups.

To interpret the significant differences between NC and PDD, we introduce here an assumption that the rate constants of the cerebellum do not change. The results showed a significant difference for $k2_{oc}$, but no significant difference was detected for DVR. It follows that the distribution volume of the occipital cortex, i.e., $K1_{oc}/k2_{oc}$, did not experience significant changes, while the rate constants $K1_{oc}$ and $k2_{oc}$ showed differences between NC and PDD. The rate constants are represented as

$$K1 = (F/PS_1)(1-e^{-PS_1/F}) \tag{13}$$

$$k2 = \frac{PS_2}{PS_1} F(1-e^{-PS_1/F}) \tag{14}$$

where F is the blood flow rate and PS_1 and PS_2 are permeability-surface area products (PS) of the BBB for the tracer from plasma to tissue and from tissue to plasma, respectively. Therefore, differences in F may cause the differences in $K1_{oc}$ and $k2_{oc}$ observed in the present study. However, changes in cerebral blood flow will not cause significant differences in the rate constants because of the small first-pass extraction (4%) of FDOPA.[17] Thus the reasoning, from the standpoint of differences in regional cerebral blood flow, is questionable. The differences in PSs could also account for the present result. When first-pass extraction is small, the rate constants K1 and k2 are approximately equal to the PS of the BBB.[17] The PSs of FDOPA and 3OMFD across the BBB are known to be mediated by the large neutral amino acid (LNAA) transport system.[21] The rate constant across the BBB follows the Michaelis-Menten equation because all LNAAs share the same LNAA transport carriers for transport across the BBB.[21] Thus the rate constants across the BBB can be formulated as

$$K1_i = \frac{Vm_i / Km_i}{1+\sum_k ([AA]_k^{plasma} / Km_k)} \tag{15}$$

and

$$k2_i = \frac{Vm_i / Km_i}{1+\sum_k ([AA]_k^{tissue} / Km_k)} \tag{16}$$

where $[AA]_k^{plasma}$ and $[AA]_k^{tissue}$ are the plasma and tissue concentrations (nmol/mL) of large neutral amino acids ($LNAA_k$), respectively; Vm_i and Km_i are, respectively, the maximal rate (nmol min^{-1} g^{-1}) and half-saturation concentration (nmol/mL) of $LNAA_i$ for the transport carrier.[21] According to Eqs. 15 and 16, the rate constants K1 and k2 depend on the regional Vmi, Kmi, and LNAA concentrations in plasma and tissue. Among these elements, the plasma LNAA concentration will be almost the same throughout the whole brain. However, other elements may vary based on metabolic circumstances. Thus, previously reported disturbances in metabolism in the occipital cortex[11-14] may have some effect on the rate constants K1 and k2 for PDD.

The population mean $\overline{k2_{Ce}}$=0.057 (min^{-1}) used in this study[16,17] may bias the results. However, even if $\overline{k2_{Ce}}$=0.04-0.07 were used, the discriminative result obtained by Dunnett's multiple comparisons test for the intercept and slope of the Logan and Patlak plots would be the same.

Although FDOPA PET may not be appropriate for investigating the occipital cortex region's disturbances in amino-acid metabolism, we still think the Logan plot has the power to confer new insights into analysis of the tracer.

Conclusion

The Logan analysis was considered to be theoretically adequate for analysis of FDOPA PET dynamic data from scan times of less than 120 min and target regions that have no irreversible compartments, e.g., occipital cortex. The Logan analysis of FDOPA PET in the occipital cortex revealed a significant difference between NC and PDD patients. It has the power to confer new insights into the analysis of FDOPA PET in regions without an irreversible compartment. As in this study, by using adequate kinetic modeling according to regional kinetic features with respect to the tracer concerned, we may obtain new insights into PET dynamic data.

References

1) Dhawan V, Ishikawa T, Patlak CS, *et al.* Combined FDOPA and 3OMFD PET studies in Parkinson's disease. *J Nucl Med,* 37: 209–216, 1996.
2) Ishikawa T, Dhawan V, Chaly T, *et al.* Clinical significance of striatal DOPA decarboxylase activity in Parkinson's disease. *J Nucl Med,* 37: 216–222, 1996.
3) Ito K, Morrish PK, Rakshi JS, *et al.* Statistical parametric mapping with ^{18}F-dopa PET shows bilaterally reduced striatal and nigral dopaminergic function in early Parkinson's disease. *J Neurol Neurosurg Psychiatry,* 66: 754–758, 1999.
4) Rakshi JS, Uema T, Ito K, *et al.* Frontal, midbrain and striatal dopaminergic function in early and advanced Parkinson's disease. A 3D[^{18}F]dopa-PET study. *Brain,* 122: 1637–1650, 1999.
5) Nagano AS, Ito K, Kato T, *et al.* Extrastriatal mean regional uptake of fluoro-18-FDOPA in the normal aged brain–an approach using MRI-aided spatial normalization. *Neuroimage,* 11: 760–766, 2000.
6) Patlak CS, Blasberg RG, Fenstermacher JD. Graphical evaluation of blood-to-brain transfer constants from multiple-time uptake data. *J Cereb Blood Flow Metab,* 3: 1–7, 1983.
7) Patlak CS, Blasberg RG. Graphical evaluation of blood-to-brain transfer constants from multiple-time uptake data generalizations. *J Cereb Blood Flow Metab,* 5: 584–590, 1985.
8) Gjedde A, Reith J, Dyve S, *et al.* Dopa decarboxylase activity of the living human brain. *Proc Natl Acad Sci U S A,* 88: 2721–2725, 1991.
9) Kuwabara H, Cumming P, Reith J, *et al.* Human striatal L-DOPA decarboxylase activity estimated in vivo using 6-[^{18}F]fluoro-DOPA and positron emission tomography: error analysis and application to normal subjects. *J Cereb Blood Flow Metab,* 13: 43–56, 1993.
10) Arahata Y, Hirayama M, Ieda T, *et al.* Parieto-occipital glucose hypometabolism in Parkinson's disease with autonomic failure. *J Neurol Sci,* 163: 119–126, 1999.
11) Imamura T, Ishii K, Sasaki M, *et al.* Regional cerebral glucose metabolism in dementia with Lewy bodies and Alzheimer's disease: a comparative study using positron emmision tomography. *Neurosci Lett,* 235: 49–52, 1997.
12) Ishii K, Imamura T, Sasaki M, *et al.* Regional cerebral glucose metabolism in dementia with Lewy bodies and Alzheimer's disease. *Neurology,* 51: 125–130, 1998.
13) Higuchi M, Tashiro M, Arai H, *et al.* Glucose hypometabolism and neuropathological correlates in brains of dementia with Lewy bodies. *Exp Neurol,* 162: 247–256, 2000.
14) Cordery RJ, Tyrrell PJ, Lantos PL, Rossor MN. Dementia with Lewy bodies studied with positron emission tomography. *Arch Neurol,* 58: 505–508, 2000.
15) McKeith IG, Galasko D, Kosaka,K, *et al.* Consensus guidelines for the clinical and pathologic diagnosis of dementia with Lewy bodies (DLB): report of the consortium on DLB international workshop. *Neurology,* 47: 1113–1124, 1996.
16) Yu DC, Huang SC, Barrio JR, Phelps ME. The assessment of the non-equilibrium effect in the 'Patlak analysis' of Fdopa PET studies. *Phys Med Biol,* 40: 1243–1254, 1995.
17) Huang SC, Yu DC, Barrio JR, *et al.* Kinetics and modeling of L-6-[^{18}F]fluoro-DOPA in human positron emission tomographic studies. *J Cereb Blood Flow Metab,* 11: 898–913, 1991.
18) Wahl L, Nahmias C. Modeling of fluorine-18-6-fluoro-L-Dopa in humans. *J Nucl Med,* 37: 432–437, 1996.
19) Logan J, Fowler JS, Volkow ND, Wang GJ, Ding YS, Alexoff DL. Distribution volume ratios without blood sampling from graphical analysis of PET data. *J Cereb Blood Flow Metab,* 16: 834–840, 1996.
20) Logan J, Fowler JS, Volkow ND, *et al.* Graphical analysis of reversible radioligand binding from time-activity measurements applied to [N-^{11}C-methyl]-(–)-cocaine PET studies in human subjects. *J Cereb Blood Flow Metab,* 10: 740–747, 1990.
21) Huang SC, Stout DB, Yee RE, Satyamurthy N, Barrio JR. Distribution volume of radiolabeled large neutral amino acids in brain tissue. *J Cereb Blood Flow Metab,* 18: 1288–1293, 1998.

PAPER

Occipital hypoperfusion in Parkinson's disease without dementia: correlation to impaired cortical visual processing

Y Abe, T Kachi, T Kato, Y Arahata, T Yamada, Y Washimi, K Iwai, K Ito, N Yanagisawa, G Sobue

J Neurol Neurosurg Psychiatry 2003;**74**:419–422

See end of article for authors' affiliations

Correspondence to: Dr Y Abe, Department of Neurology, Chubu National Hospital, Obu, Aichi 474–8511, Japan; yujiabe@chubu-nh.go.jp

Received 5 August 2002
Accepted in revised form 22 October 2002

Objective: The purpose of this study was to analyse changes in regional cerebral blood flow (rCBF) in Parkinson's disease (PD) without dementia.
Methods: Twenty eight non-demented patients with PD and 17 age matched normal subjects underwent single photon emission computed tomography with N-isopropyl-p-[^{123}I]iodoamphetamine to measure rCBF. The statistical parametric mapping 96 programme was used for statistical analysis.
Results: The PD patients showed significantly reduced rCBF in the bilateral occipital and posterior parietal cortices ($p<0.01$, corrected for multiple comparison $p<0.05$), when compared with the control subjects. There was a strong positive correlation between the score of Raven's coloured progressive matrices (RCPM) and the rCBF in the right visual association area ($p<0.01$, corrected for multiple comparison $p<0.05$) among the PD patients.
Conclusions: This study showed occipital and posterior parietal hypoperfusion in PD patients without dementia. Furthermore, it was demonstrated that occipital hypoperfusion is likely to underlie impairment of visual cognition according to the RCPM test, which is not related to motor impairment.

It has been reported in previous studies that patients with Parkinson's disease (PD), even those without dementia, showed changes in regional cerebral blood flow (rCBF).[1–4] However, the findings of these investigations have been inconsistent. Frontal[1 2] parietal,[3], temporal,[4] or global[1 5] cortical hypoperfusion, or unchanged blood flow[4–8] have been reported. This inconsistency is considered to be attributable, not only to the heterogeneity among PD patients, but also to the lack of standardisation of image-analysing methods. In most previous studies, visually placed region of interest (ROI) analysis methods were used to evaluate the alterations of rCBF. This approach is limited in that the manual placement of ROI gives rise to the observer biases and large areas of the brain are left unexplored.

Statistical parametric mapping (SPM), developed by Frinston *et al*, is a voxel based statistical technique that is used to examine regional changes in imaging data.[9 10] This is entirely automated and objective, and can completely overcome the disadvantage of earlier ROI analysis methods. Recently, the SPM programme has been widely used to examine regional dysfunction of the brain in various neurological diseases.[5 11–13]

The purpose of this study was to analyse the rCBF in PD patients without dementia on a voxel by voxel basis using single photon emission computed tomography (SPECT) with N-isopropyl-p-[^{123}I]iodoamphetamine (^{123}I-IMP) and the SPM programme. We compared the rCBF in PD patients to that in age matched normal subjects. In addition, we investigated the relation between the rCBF and clinical features in PD patients.

Table 1 Clinical features of subjects

	Normal controls (n=17)	Patients with Parkinson's disease (n=28)
Age (y)*	69.6(10.2)	67.3 (7.3)
Sex (F/M)	9/8	17/11
Duration of illness (y)*		8.6 (4.6)
UPDRS motor score*		35.2 (12.9)

*Mean (SD).

METHODS

Subjects

Twenty eight PD patients without dementia and 17 age matched normal control subjects were included in this study (table 1). The 28 PD patients were diagnosed with the United Kingdom Parkinson's Disease Society Brain Bank criteria for clinical diagnosis of idiopathic PD,[14] and the extrapyramidal symptoms were scored according to the motor examination score of the Unified Parkinson's Disease Rating Scale (UPDRS).[15] Patients who had visual hallucination were excluded. No abnormal intensity or obvious cortical atrophy was seen on magnetic resonance imaging of the brain of any patient. None of the patients had any other illnesses or were taking any medication, except for antiparkinsonian drugs. All 28 patients had been taking levodopa treatment at the time of SPECT scanning. In addition, dopamine receptor agonists had been used in 12 patients, six patients had been treated with low dose anticholinergic agents, droxydopa had been given to two patients, and three patients had been taking amantadine hydrochloride.

None of the 17 normal control subjects had a history of any neurological or psychiatric disorders, and the neurological examination of each control subject was normal.

All of the PD and control subjects were assessed using the mini-mental state examination (MMSE),[16] and 25 PD patients and 14 control subjects also took the Raven's coloured progressive matrices (RCPM).[17] For both SPECT scanning and cognitive test, all patients were examined after overnight withdrawal of medication.

Informed consent was obtained from every subject before the study. Permission to perform this study was obtained from the ethical committee of Chubu National Hospital.

Abbreviations: PD, Parkinson's disease; rCBF, regional cerebral blood flow; RCPM, Raven's coloured progressive matrices; MMSE, mini-mental state examination; ROI, region of interest; SPM, statistical parametric mapping

Image acquisition

^{123}I-IMP (Nihon Mediphysics, Hyogo, Japan), 222 MBq (6 mCi), was injected into an antecubital vein while the subjects laid in a supine position with eyes closed in a quiet room. A single blood sample was obtained from the brachial artery between 9 and 10 minutes after the ^{123}I-IMP administration. SPECT scanning was carried out between 15 and 45 minutes after injection using a two head rotating GCA 7200DI gammacamera (Toshiba, Tokyo, Japan) fitted with low energy, high resolution collimators. The data were acquired in a 128×128 matrix through a 180° rotation at an angle interval of 4°. The projection data were prefiltered through a Butterworth filter, and then reconstructed using a Ramp backprojection filter. Chang's attenuation correction[18] and scattering correction using the triple energy window method[19] were applied to the reconstructed images. The in-plane spatial resolution was 11.1 mm in full width at half maximum (FWHM). The final image slices were set up parallel to the orbitomeatal line and were obtained at an interval of 3.44 mm through the entire brain. The rCBF images were quantitated according to the IMP-ARG method.[20] This method is based on the two compartment model for tracer kinetics, and uses a standard arterial input calibrated by the radioactivity of a single arterial whole blood sample, a standard lipophilic fraction of ^{123}I-IMP in whole blood and fixed distribution volume of ^{123}I-IMP. All images were transferred to a Sun workstation (Sun Microsystems, Mountain View, CA, USA) for further analysis.

Data analysis

The data were analysed using the statistical parametric mapping 96 (SPM96; Wellcome Department of Cognitive Neurology, Institute of Neurology, London, UK)[9 10] implemented in MATLAB (Math Works, Sherborn, MA, USA). Each image was transformed into the standard anatomical space with the programme provided by the Montreal Neurological Institute.[21] All of the images resulting from the normalisation procedure were visually acceptable. The global CBF of PD patients was 49.5 (9.9) ml/100g/min (mean (SD)), and that of normal controls was 52.4 (13.1) ml/100g/min. There was no significant difference of the mean global CBF in the two groups, but the apparent interindividual variation of the global CBF was seen in each group. Therefore, in the following analyses, proportional scaling was applied to adjust the mean whole brain activity to 50 ml/100 g/min to avoid interindividual variation in global CBF. The grey matter threshold was 0.8.

For comparison between the PD group and the control group, the normalised images of the non-demented patients with PD and those of the normal subjects were compared by a voxel by voxel *t* statistics. The resulting statistical parametric maps of *t* statistics, SPM{t}, were transformed to maps of the unit normal distribution, SPM{z}. The statistical significance was chosen at a level of $z>2.33$ (equivalent to an uncorrected $p<0.01$). To correct for multiple comparisons, the significance of the difference between each detected brain region was estimated using distributional approximations from theory of Gaussian field, in terms of spatial extent and peak height. A corrected p value of 0.05 was used as the final threshold for significance.

Next, we compared the images of the PD patients to examine whether there were any voxels in which the rCBF was significantly correlated with various clinical characteristics including the duration of illness, the UPDRS motor score, the MMSE score, and the RCPM score. Each value of the clinical characteristics was used as a covariate of interest, and both the values of the global rCBF and age were used as confounding covariates. The statistical significance was chosen at a level of $z>2.33$ (equivalent to an uncorrected $p<0.01$). A corrected p value of 0.05 was chosen in multiple comparisons.

Table 2 Brain regions in which the rCBF of the PD group was significantly lower than that of the normal control group (SPM analysis)

Cerebral region	Brodmann's area	x	y	z	Z
L middle occipital gyrus	18, 19, 39	-34	-78	8	4.63
R middle occipital gyrus	18, 19, 39	28	-84	14	4.28
L angular gyrus	39	-46	-54	34	3.43
R angular gyrus	39	44	-56	38	3.98
L cuneus	18	-26	-86	0	3.37
R cuneus	18	8	-88	14	2.57
L calcarine sulcus	17	-18	-94	-8	3.69
L precuneus	7	-10	-70	42	3.37
L lingual gyrus	18	-18	-84	-16	3.36
L superior occipital gyrus	19	-32	-84	30	3.34
L superior parietal lobule	7	-12	-72	52	3.23

x, y, z=coodinates of the peak in the standard anatomical space; Z=Z score of maximal peak; L=left; R=right. $p<0.01$, corrected for multiple comparisons.

RESULTS

Clinical manifestations

The total UPDRS motor examination score ranged from 3 to 56, and the mean (SD) score was 34.8 (13.2). The mean MMSE score of the 28 PD patients was 28.1 (2.1) (range, 25 to 30), and that of the 17 control subjects was 28.5 (2.0) (range, 25 to 30). The MMSE score of the PD group did not differ significantly from that of the control group. The mean RCPM score was 24.4 (5.2) (range, 16 to 33) for the 25 PD patients, and was 28.2 (3.5) (range, 25 to 34) for the 10 control subjects. The RCPM score of the PD group was significantly lower than that of the control group ($p<0.05$).

There was no correlation between the age, the duration of illness, the UPDRS motor examination score, the MMSE score, and the RCPM score in the PD group.

Comparison of the rCBF between the PD and normal control groups

Twenty eight PD patients without dementia and 17 control subjects underwent SPECT scanning, and the images of the PD and control groups were compared. According to SPM analysis, the rCBF in the bilateral occipital cortices and the bilateral posterior parietal cortices in the PD group were significantly lower than those in the respective area in the control group ($p<0.01$, corrected $p<0.05$) (table 2, fig 1).

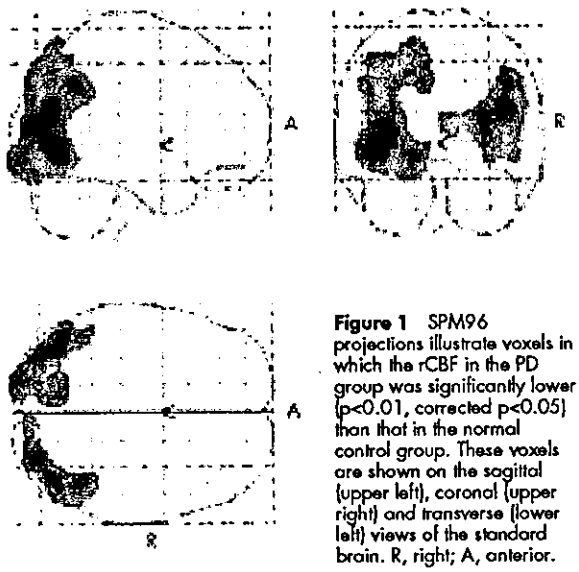

Figure 1 SPM96 projections illustrate voxels in which the rCBF in the PD group was significantly lower ($p<0.01$, corrected $p<0.05$) than that in the normal control group. These voxels are shown on the sagittal (upper left), coronal (upper right) and transverse (lower left) views of the standard brain. R, right; A, anterior.

Table 3 Brain regions in which there was a positive correlation between the RCPM score and the rCBF among 25 PD patients (SPM analysis)

Cerebral region	Brodmann's area	x	y	z	Z
R angular gyrus	39	46	−66	24	4.36
R middle occipital gyrus	19	40	−70	18	4.34
R inferior parietal lobule	40	42	−50	46	3.09

x, y, z=coodinates of the peak in the standard anatomical space; Z=Z score of maximal peak; R=right. p<0.01, corrected for multiple comparisons.

There was no brain region in which the rCBF was significantly higher in the PD group than in the control group.

Correlation between clinical characteristics and rCBF in the PD patients without dementia

There was a positive correlation between the RCPM score and the rCBF in the right dorsolateral occipital and the right posterior parietal cortices ($p<0.01$, corrected $p<0.05$) among 25 PD patients (table 3, fig 2). In most of these regions, the rCBF was reduced significantly in the PD group compared with the normal control group. There was no correlation between the duration of illness, the UPDRS motor examination score, or the MMSE score and the value of rCBF for any brain region.

DISCUSSION

This study showed that the rCBF in the non-demented PD patients was significantly lower than that in the age matched normal subjects in the bilateral occipital and posterior parietal cortices. It is well known that patients with PD, even those who do not have dementia, often develop various kinds of cognitive abnormalities that are closely related to visual dysfunction. Loss of luminance and colour contrast sensitivity and the impairment in preattentive cortical visual processing have been reported.[22-24] Furthermore, neuropsychological studies have revealed that PD patients have visuospatial deficit.[25 26] It seems appropriate to conclude that occipital dysfunction is a common feature of PD patients without dementia.

Actually, in our study, the mean RCPM score in the PD group was significantly lower than that in the normal control group, although the MMSE score of the PD group and that of the control group did not differ. RCPM is used for evaluation of visual perception, especially visuospatial attention, as the person taking the test must visually analyse form, colour, and linear slope.[27] Moreover, RCPM is one of the most appropriate batteries to test visual perceptual function purely, because it requires very little motor response. Therefore, in PD patients, the RCPM score is not likely to be affected by the poor motor ability. In fact, the RCPM score did not correlate to the UPDRS motor score in our PD patients. The impairment in RCPM test is clearly distinct from dementia, and is not considered to be secondary to the motor dysfunction.

In this study, we found that there was a strong positive correlation between the RCPM score and the rCBF in the right dorsolateral occipital area, corresponding to the visual association cortex, and the right posterior parietal area among non-demented PD patients. In these areas, there was no correlation between the UPDRS motor score and the rCBF, therefore, it may be reasonable to suppose that the reduction of rCBF in the visual association area purely reflects the impairment in cortical visual processing. Although some previous studies demonstrated occipital hypoperfusion and glucose hypometabolism,[5 28-31] there has been no previous study showing that the correlation between occipital hypometabolism or hypoperfusion and clinical abnormality related with visual

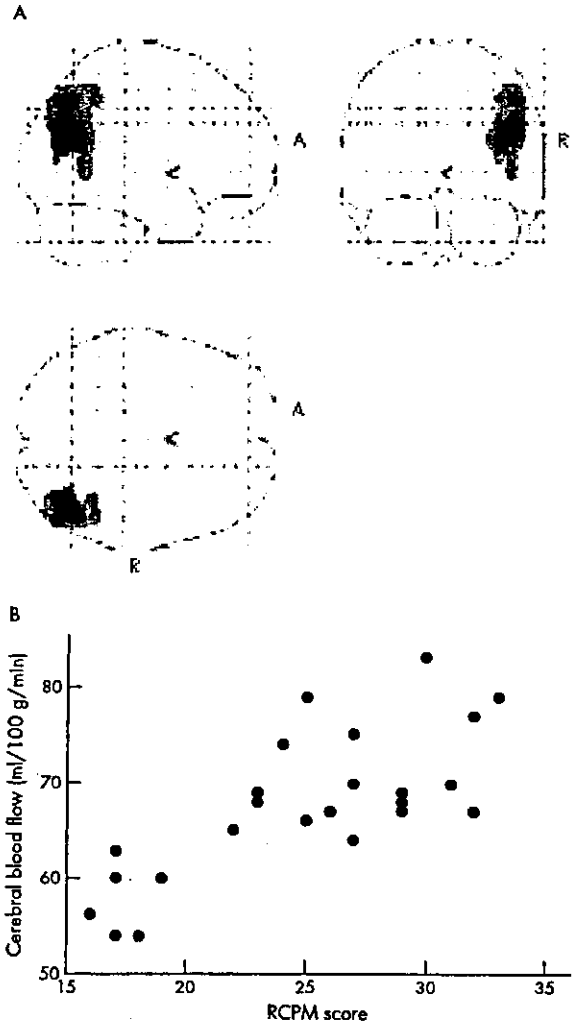

Figure 2 (A) SPM96 projections illustrate voxels in which there is a positive correlation ($p<0.01$, corrected $p<0.05$) between the RCPM score and the rCBF among 25 PD patients. R, right; A, anterior. (B) Scatter plot between the RCPM score and the rCBF at the voxel in the right middle occipital gyrus where there is a positive correlation ($p<0.005$, $r=0.73$, Spearman's correlation coefficient by ranks) between the RCPM score and the rCBF. *The mean whole brain activity was adjusted to 50 ml/100 g/min.

dysfunction was directly proved. This is the first study to demonstrate this correlation. The reason why the correlation was seen only in the right hemisphere is not clear, but this is possibly associated with the dominance of the right hemisphere in visuospatial attention.[32 33]

The underlying mechanism of the reduction of rCBF in the occipital lobe of PD patients remains unknown. In the previous report, a reduction of amplitude in the pattern electroretinogram[34] was demonstrated in PD patients. This abnormality has been considered to be attributable to diminished dopaminergic neurons in the retina, and this retinal dysfunction may be responsible for the occipital hypoperfusion. Furthermore, PD patients may have primary pathological findings in the cortices. However, morphological studies have not disclosed primary abnormalities, such as neuronal loss, gliosis, and appearance of Lewy bodies, in these brain regions in non-demented PD patients.[35 36] Another explanation, which seems much more plausible, is a functional deficit of the cortex that results from damage to the

subcortical structure. There is considerable evidence supporting the presence of a corticostriatal projection which arises from the entire cortical region and projects to the striatum.[37 38] The compact zone of the substantia nigra also gives off efferents to the striatum, and is widely believed to modify the activity of the cortical output to the striatum.[37 39] Therefore, the loss of nigrostriatal neurons may impair the association between the cortical region and the striatum, and consequently may reduce cortical activity. The research group of Denny-Brown and Yanagisawa reported the intimate functional connection between the visual association areas and the striatum.[39 40] They demonstrated in monkeys that extensive destruction of the posterior part of the putamen was followed by a remarkable loss of visual attention and inhibition of grasp and traction response, and that these signs also resulted from destruction of the visual association cortex and the posterior parietal cortex. The physical connection of the visual association cortex and the posterior parietal cortex with the posterior part of the putamen was also described by Kemp and Powell.[41]

It is difficult to detect the correlation between RCPM score and the rCBF in the dorsolateral visual association areas, if conventional ROI analysis methods had been used. Because the dorsolateral visual association area is located around the parieto-occipital junction, most investigators avoid setting of ROIs in this area. On the other hand, using the SPM program, whole brain lesions can be explored by a voxel based statistical technique. It has become possible using the SPM program to detect that occipital hypoperfusion is related to the visual dysfunction according to the RCPM test.

In conclusion, we confirmed that occipital hypoperfusion is a common feature of PD patients without dementia. It was demonstrated that occipital hypoperfusion is likely to reflect the visual impairment examined with the RCPM test that is not related to the motor impairment.

Authors' affiliations
Y Abe, K Iwai, G Sobue, Department of Neurology, Nagoya University School of Medicine, Nagoya, Japan
Y Abe, T Kachi, Y Arahata, T Yamada, Y Washimi, K Iwai, Department of Neurology, Chubu National Hospital, Aichi, Japan
T Kato, K Ito, Department of Biofunctional Research, National Institute for Longevity Sciences, Aichi, Japan
N Yanagisawa, Department of Neurology, Kanto Rosai Hospital, Kanagawa, Japan

Funding: this research was partly supported by a Health Sciences Research Grant for Comprehensive Research on Aging and Health and a Health Sciences Research Grant for Research on Brain Science from the Ministry of Health, Labour and Welfare of Japan.

Competing interests: none declared.

REFERENCES

1 **Wolfson LI,** Leenders KL, Brown LL, *et al.* Alterations of regional cerebral blood flow and oxygen metabolism in Parkinson's disease. *Neurology* 1985;**35**:1399–405.
2 **Defebvre L,** Lacouffe P, Destee A, *et al.* Tomographic measurements of regional cerebral blood flow in progressive supranuclear palsy and Parkinson's disease. *Acta Neurol Scand* 1995;**92**:235–41.
3 **Tachibana H,** Kawabata K, Tomino Y, *et al.* Brain perfusion imaging in Parkinson's disease and Alzheimer's disease demonstrated by three-dimensional surface display with 123I-iodoamphetamine. *Dementia* 1993;**4**:334–41.
4 **Jagust WJ,** Reed BR, Martin EM, *et al.* Cognitive function and regional cerebral blood flow in Parkinson's disease. *Brain* 1992;**115**:521–37.
5 **Imon Y,** Matsuda H, Ogawa M, *et al.* SPECT image analysis using statistical parametric mapping in patients with Parkinson's disease. *J Nucl Med* 1999;**40**:1583–9.
6 **Perlmutter JS,** Raichle ME. Regional blood flow in hemiparkinsonism. *Neurology* 1985;**35**:1127–34.
7 **Spampinato U,** Habert MO, Mas JL, *et al.* [^{99m}Tc]-HM-PAO SPECT and cognitive impairment in Parkinson's disease: a comparison with dementia of the Alzheimer type. *J Neurol Neurosurg Psychiatry* 1991;**54**:787–92.
8 **Wang SJ,** Liu RS, Liu HC, *et al.* Technetium-99m hexamethylpropylene amine oxime single photon emission tomography of the brain in early Parkinson's disease: correlation with dementia and lateralization. *Eur J Nucl Med* 1993;**20**:339–44.
9 **Friston KJ,** Ashburner J, Frith CD, *et al.* Spatial registration and normalization of images. *Hum Brain Mapp* 1995;**3**:165–89.
10 **Friston KJ,** Holmes AP, Worsley KJ, *et al.* Statistical parametric maps in functional imaging: a general linear approach. *Hum Brain Mapp* 1995;**2**:189–210.
11 **Roelcke U,** Kappos L, Lechner-Scott J, *et al.* Reduced glucose metabolism in the frontal cortex and basal ganglia of multiple sclerosis patients with fatigue: a ^{18}F-fluorodeoxyglucose positron emission tomography study. *Neurology* 1997;**48**:1566–71.
12 **Desgranges B,** Baron JC, de la Sayette V, *et al.* The neural substrates of memory systems impairment in Alzheimer's disease. A PET study of resting brain glucose utilization. *Brain* 1998;**121**:611–31.
13 **Van Bogaert P,** David P, Gillain CA, *et al.* Perisylvian dysgenesis. Clinical, EEG, MRI and glucose metabolism features in 10 patients. *Brain* 1998;**121**:2229–38.
14 **Hughes AJ,** Daniel SE, Kilford L, *et al.* Accuracy of clinical diagnosis of idiopathic Parkinson's disease: a clinico-pathological study of 100 cases. *J Neurol Neurosurg Psychiatry* 1992;**55**:181–4.
15 **Fahn S,** Elton RL, Members of the UPDRS Development Committee. Unified Parkinson's disease rating scale. In: Fahn S, Marsden CD, Calne DB, *et al*, eds. *Recent development in Parkinson's disease.* Florham Park NJ: MacMillan Healthcare Information, 1987:153–63, 293–304.
16 **Folstein MF,** Folstein SE, McHugh PR. "Mini-mental state". A practical method for grading the cognitive state of patients for the clinician. *J Psychiatr Res* 1975;**12**:189–98.
17 **Raven J.** *Guide to using the coloured progressive matrices.* London: Lewis, 1965.
18 **Chang LT.** A method for attenuation correction in radionuclide computed tomography. *IEEE Trans Nucl Sci* 1978;**25**:638–43.
19 **Ogawa K.** A practical method for position-dependent compton-scatter correction in single photon emission CT. *IEEE Trans Med Imaging* 1991;**10**:408–12.
20 **Iida H,** Itoh H, Nakazawa M, *et al.* Quantitative mapping of regional cerebral blood flow using iodine-123-IMP and SPECT. *J Nucl Med* 1994;**35**:2019–30.
21 **Evans AC,** Collins DL, Milner B. An MRI-based stereotactic atlas from 250 young normal subjects. *Soc Neurosci Abstr* 1992;**18**:408.
22 **Bodis-Wollner I,** Marx MS, Mitra S, *et al.* Visual dysfunction in Parkinson's disease. Loss in spatiotemporal contrast sensitivity. *Brain* 1987;**110**:1675–98.
23 **Haug BA,** Kolle RU, Trenkwalder C, *et al.* Predominant affection of the blue cone pathway in Parkinson's disease. *Brain* 1995;**118**:771–8.
24 **Lieb K,** Brucker S, Bach M, *et al.* Impairment in preattentive visual processing in patients with Parkinson's disease. *Brain* 1999;**122**:303–13.
25 **Pirozzolo FJ,** Hansch EC, Mortimer JA, *et al.* Dementia in Parkinson disease: a neuropsychological analysis. *Brain Cogn* 1982;**1**:71–83.
26 **Boller F,** Passafiume D, Keefe NC, *et al.* Visuospatial impairment in Parkinson's disease. Role of perceptual and motor factors. *Arch Neurol* 1984;**41**:485–90.
27 **Tanaka F,** Kachi T, Yamada T, *et al.* Auditory and visual event-related potentials and flash visual evoked potentials in Alzheimer's disease: correlations with Mini-Mental State Examination and Raven's coloured progressive matrices. *J Neurol Sci* 1998;**156**:83–8.
28 **Peppard RF,** Martin WR, Carr GD, *et al.* Cerebral glucose metabolism in Parkinson's disease with and without dementia. *Arch Neurol* 1992;**49**:1262–8.
29 **Eberling JL,** Richardson BC, Reed BR, *et al.* Cortical glucose metabolism in Parkinson's disease without dementia. *Neurobiol Aging* 1994;**15**:329–35.
30 **Bohnen NI,** Minoshima S, Giordani B, *et al.* Motor correlates of occipital glucose hypometabolism in Parkinson's disease without dementia. *Neurology* 1999;**52**:541–6.
31 **Hu MT,** Taylor-Robinson SD, Chaudhuri KR, *et al.* Cortical dysfunction in non-demented Parkinson's disease patients: a combined ^{31}P-MRS and ^{18}FDG-PET study. *Brain* 2000;**123**:340–52.
32 **Warrington EK,** James M, Kinsbourne M. Drawing disability in relation to laterality of cerebral lesion. *Brain* 1966;**89**:53–82.
33 **Benson DF,** Barton MI. Disturbances in constructional ability. *Cortex* 1970;**6**:19–46.
34 **Ikeda H,** Head GM, Ellis CJ. Electrophysiological signs of retinal dopamine deficiency in recently diagnosed Parkinson's disease and a follow up study. *Vision Res* 1994;**34**:2629–38.
35 **Jellinger KA.** Pathology of Parkinson's disease. Changes other than the nigrostriatal pathway. *Mol Chem Neuropathol* 1991;**14**:153–97.
36 **Hughes AJ,** Daniel SE, Blankson S, *et al.* A clinicopathologic study of 100 cases of Parkinson's disease. *Arch Neurol* 1993;**50**:140–8.
37 **Alexander GE,** Crutcher MD. Functional architecture of basal ganglia circuits: neural substrates of parallel processing. *Trends Neurosci* 1990;**13**:266–71.
38 **Parent A,** Hazrati LN. Functional anatomy of the basal ganglia. I. The cortico-basal ganglia-thalamo-cortical loop. *Brain Res Brain Res Rev* 1995;**20**:91–127.
39 **Denny-Brown D,** Yanagisawa N, Kirk E. The localization of hemispheric mechanism of visually directed reaching and grasping. In: Zülch KJ, Kreutzfeldt O, Galbraith GC, eds. *Cerebral localization.* Berlin: Springer, 1975:62–75.
40 **Denny-Brown D,** Yanagisawa N. The role of the basal ganglia in initiation of movement. In: Yahr M, ed. *The basal ganglia.* New York: Raven Press, 1976:115–49.
41 **Kemp JM,** Powell TP. The cortico-striate projection in the monkey. *Brain* 1970;**93**:525–46.

Evaluation of 5-^{11}C-Methyl-A-85380 as an Imaging Agent for PET Investigations of Brain Nicotinic Acetylcholine Receptors

Yasuhiko Iida, PhD[1]; Mikako Ogawa, MS[2]; Masashi Ueda, MS[1]; Akiko Tominaga, MS[1]; Hidekazu Kawashima, PhD[1]; Yasuhiro Magata, PhD[2]; Shingo Nishiyama, MS[3]; Hideo Tsukada, PhD[3]; Takahiro Mukai, PhD[4]; and Hideo Saji, PhD[1]

[1]Department of Patho-Functional Bioanalysis, Graduate School of Pharmaceutical Sciences, Kyoto University, Kyoto, Japan; [2]Laboratory of Genome Bio-Photonics, Photon Medical Research Center, Hamamatsu University School of Medicine, Hamamatsu, Japan; [3]Central Research Laboratory, Hamamatsu Photonics K.K., Hamamatsu, Japan; and [4]Department of Nuclear Medicine, Graduate School of Medicine, Kyoto University, Japan

Central nicotinic acetylcholine receptors (nAChRs) represent major neurotransmitter receptors responsible for various brain functions, and changes in the density of nAChRs have recently been reported in several neurodegenerative diseases. Visualization of nAChRs in human brain has thus been of great interest, and the development of radiopharmaceuticals for the imaging and quantitative assessment of central nAChRs has been desired. In this study, we synthesized 5-^{11}C-methyl-3-(2-(S)-azetidinylmethoxy)pyridine (5MA), a derivative of 3-(2-(S)-azetidinylmethoxy)pyridine (A-85380) ^{11}C-methylated at position 5 of the pyridyl fragment, and evaluated its potential for investigating central nAChRs by PET. **Methods:** ^{11}C-5MA was synthesized by the incorporation of ^{11}C-methyl iodide into 5-butylstannyl A-85380, using a Pd-catalyzed coupling reaction. The affinity of 5MA for central nAChRs was measured by displacement of (−)-^{3}H-cytisine from binding sites in rat cortical membranes. The biodistribution of ^{11}C-5MA was determined with mice. PET studies were performed on rhesus monkeys with a high-resolution PET scanner for animals. **Results:** The overall synthesis time was 60 min from the end of radionuclide production, and the radiochemical yield, after purification by high-performance liquid chromatography, was 30%. The radiochemical purity of the product was >99%, with a specific radioactivity of >36 GBq/μmol. In vitro receptor-binding assays demonstrated that 5MA has a high, selective binding affinity for nAChRs, being approximately 1.5-fold higher than that of A-85380, 3.5-fold higher than that of (−)-cytisine, and 10-fold higher than that of (−)-nicotine. The distribution studies in mice showed that the brain uptake of ^{11}C-5MA was profound. Regional cerebral distribution studies in mice demonstrated that the accumulation of ^{11}C-5MA was consistent with the density of nAChRs, with the highest uptake observed in the thalamus, a moderate uptake in the cortex and striatum, and the lowest uptake in the cerebellum. Furthermore, preinjection of nAChR-binding ligands, (−)-nicotine and (−)-cytisine, reduced the uptake of ^{11}C-5MA in brain regions of high uptake in the untreated experiment. PET imaging studies with ^{11}C-5MA in rhesus monkeys demonstrated clear images consistent with the distribution of nAChRs in the brain. **Conclusion:** These results suggest that ^{11}C-5MA is a potential PET radiopharmaceutical for nuclear medical studies of nAChRs in the brain.

Key Words: central nicotinic acetylcholine receptors; 5-^{11}C-methyl-3-(2-(S)-azetidinylmethoxy)pyridine; receptor-binding affinity; biodistribution; PET

J Nucl Med 2004; 45:878–884

Nicotinic acetylcholine receptors (nAChRs) have been implicated in a variety of brain functions and behavioral states, including learning, memory, attention, and anxiety (*1–4*). Furthermore, a decrease in central nAChRs has been observed in several neurodegenerative diseases, including Alzheimer's disease (*5–8*) and Parkinson's disease (*9,10*). In addition, increases in nAChRs have been observed in the brains of smokers (*11*).

Thus, imaging for nAChRs in the brain with PET or SPECT has been of great interest for the evaluation of brain functions and diagnosis of neurodegenerative diseases. For this purpose, several radiotracers for PET or SPECT of nAChRs have been developed (*12–16*). Among these compounds, ^{18}F-fluorinated and ^{123}I-iodinated derivatives of 3-(2-(*S*)-azetidinylmethoxy)pyridine (A-85380) are promising because of their high, selective affinity for $\alpha_4\beta_2$, the predominant subtype of nAChR in the brain, high cerebral accumulation, and low toxicity (*12,17–27*).

5-Methyl-3-(2-(*S*)-azetidinylmethoxy)pyridine (5MA), an A-85380 derivative methylated at position 5 of the pyridyl fragment, has recently been reported to have high affinity for nAChRs (*28*). In this study, ^{11}C-5MA was synthesized and its receptor-binding affinity, biodistribution in rodents, and imaging with PET in rhesus monkeys were investigated to evaluate its potential for investigating central nAChRs by PET.

Received Oct. 7, 2003; revision accepted Dec. 29, 2003.

For correspondence or reprints contact: Hideo Saji, PhD, Department of Patho-Functional Bioanalysis, Graduate School of Pharmaceutical Sciences, Kyoto University, Sakyo-ku, Kyoto 606-8501, Japan.
E-mail: hsaji@pharm.kyoto-u.ac.jp